INTERNATIONAL JOURNAL OF
COASTAL & OFFSHORE ENGINEERING IJCOE Vol.6/No.5 /Autumn 2021 (64-75) / **Special issue of "Marine Renewable Energy"**

Available online at: www. Ijcoe.org

Evaluation of SSG breakwaters on the southern shores of the Caspian Sea to produce sustainable energy

Milad Raoufi[1], Payam Zanganeh Ranjbar[2*], Mirabdolhamid Mehrdad[3]

[1] *MSc in civil engineering, Department of Civil Engineering, Faculty of Engineering, University of Guilan, P.O. 3756, Rasht, Guilan, Iran; R.milad24@gmail.com*
[2*] *Assistant Professor, Department of Civil Engineering, Faculty of Engineering, University of Guilan, P.O. 3756, Rasht, Guilan, Iran; P.zanganeh@guilan.ac.ir*
[3] *Associate Professor, Department of Civil Engineering, Faculty of Engineering, University of Guilan, P.O. 3756, Rasht, Guilan, Iran; Mehrdad@guilan.ac.ir*

ARTICLE INFO

Article History:
Received: 02 July 2021
Accepted: 10 Oct 2021

Keywords:
Caspian Sea
SSG breakwater
Wave energy
Marine energy

ABSTRACT

In this research, objecting to the use of a lesser-known type of energy source, marine wave potential, the application of Sea-wave Slot-cone Generator (SSG) breakwater was investigated in the Caspian Sea. This study had two main objectives. 1) Investigation of the conditions of each of the selected waves in terms of speed factor in the face of this breakwater 2) Investigation of the scattering of different waves in the Bandar Anzali area on the southern shores of the Caspian Sea. About the first goal, eight waves with different characteristics were selected and applied. According to the simulation results, the wave with a height of 2.825 meters and speed of 6.56 m/s and waves with a height of 0.5 and 2.825 meters and speed of 13.02 m/s, with an efficiency of more than 50%, had the highest efficiency among the simulated waves. Nevertheless, in connection with the second goal, by examining the wave height diagram and the diagram of the specified wave period, most of the waves that occurred in the Bandar Anzali region in 100 days are close to the wave with a height of 0.5 meters and speed of 6.56 m/s with an efficiency of about 7%. It does not have an opinion, and the number of waves that occurred with favorable conditions is less than expected. Therefore, it was found that the use of SSG breakwater in Anzali port located on the southern shores of the Caspian Sea is not economically viable.

1.Introduction

The world has always needed more energy resources as it progresses. Humankind has tried to use knowledge to reduce these destructive effects, as exemplified by renewable energy use. Energies such as wind energy, solar energy, marine energy, etc., are examples of these efforts. Unlike fossil fuels, these energies are much less polluting and more stable than they are. In all societies, sustainable energy sources are essential because sustainable development will cover these sustainable sources.

One group of renewable energies that is less studied than other energies is marine energy. Oceans, seas, lakes, rivers, etc., are considered as sources of this energy. Among the types of energies related to marine energy, we can mention the energy of sea currents, wave energy, geothermal energy, tidal energy, salinity gradient energy, etc.

In this study, the use of SSG breakwater has been investigated. This breakwater has different types such as three-tank, two-tank, and single-tank models. These models have also been studied on different slopes. In this research, the three-tank model has been used.

This study aims to evaluate the feasibility of using SSG breakwater in the Bandar Anzali region on the southern shores of the Caspian Sea. In the first part, the general situation of the Caspian Sea is explained. The second part deals with building a model for the desired simulation and the explanations around it. In the third section, the results obtained from each simulation step are discussed. Also, sections four and five deal with the discussion and conclusions about the issues raised.

In 2005, j.kofoed experimentally tested a three-tank model of the SSG breakwater installed on an island in Norway[1]. Larsen and Kofoed investigated surface loads caused by waves in the SSG breakwater, exposed to high waves[2]. In a study, Kofoed et al. Examined the wave conditions at the SSG breakwater prototype's installation site in the Kuwaiti region of

Norway. The MildSim computer model was also used in this study to obtain a realistic combination of wave conditions[3]

In 2006, Kofoed et al. Investigated dynamic wave loading on the SSG breakwater, which observed two types of behavior. Behavior on the sloping front plates was accompanied by a surge and an action on the vertical rear walls in the upper tank associated with a weak water jet[4]

Jensen et al. Presented a report in 2006 for the SSG breakwater, which was a series of overflows in tanks and power generated by turbines. This report aimed to enable the user to optimize the geometry and program of the turbine. Simulate, and in fact, this report was like a manual guide to generating power from the SSG breakwater[5]. In another study, Beseau investigated the application of computational fluid dynamics (CFD) to wave loading in SSG breakwaters, and the CFX10 method was used to generate strong waves[6]. In a 2007 study, Margheritini investigated the general forces acting on an SSG converter structure in 3D. The results were presented in terms of maximum forces in three different directions and application points related to the system[7]. In an article, Borgorino and Kofoed reported on the steps in setting up an SSG converter at a Lisle site[8]. Margheritini et al. Wrote an article in 2009 describing the status and performance of the SSG breakwater. Finally, three tanks were provided for it. Besides, the front panels have an angle of 35 degrees[9]. In a 2014 study, Alamian et al. Examined different converters to find suitable converters for the Caspian Sea[10]. Oliviera et al. Investigated the effect of wave focuses walls on an SSG converter's performance. These members concentrate the energy of the random waves and thus increase the overtopping phenomenon[11]

Mariano Buccino et al. in their research Used computational fluid dynamics (CFD) in SSG converters in 17 experiments[12]. In another study in 2017, Musa et al. Validated numerical models against physical experiments[13]. Yazid Maliki et al. Examined the possibility of using CFDs for large-scale wave converter (WEC) simulations. This study aimed to validate the use of CFD simulation[14]. Salimi et al. Examined the possibility of using this breakwater in the Oman Sea and the Persian Gulf[15]. In another 2019 study, Rodriguez Delgado et al. Examined the effects of rising sea levels on a wave farm's performance to protect the coast from shoreline erosion, in which they explored several scenarios[16]. Di Lauro et al. in 2020 analyzed a model of an overpass breakwater called the OBREC-V that examined hydraulic efficiency and response stability against hydraulic loads[17]. In a study, Hernandez-Fontes et al. Examined social, economic, and environmental factors surrounding ocean energy use in areas without electricity[18] Gonçalves et al .in 2020, using 30-year hindcast and previous studies in the Canary Islands to study the wave climate for more ccurate wave energy information to get a more comprehensive view of the energy sources of the waves[19]. Ribal et al. in a research explored the high potential of wave energy off the coast of Indonesia[20]. In 2020, Alizadeh et al. Examined the spatiotemporal variability of wave power in the Persian Gulf by the end of the 21st century[21]. Jahangir et al. Also investigated an energy/wind turbine/wave converter system in the Iranian seas[22].

1. Caspian sea

With 371,000 square kilometers, the Caspian Sea is located between southeastern Europe and Asia at latitudes of 47.13 and 36.34 latitude and 46.43 and 54.51 longitude. Countries around the Caspian Sea include Russia, Azerbaijan, Iran, Turkmenistan, and Kazakhstan. In terms of climate, the Caspian Sea generally has a windy environment that provides ideal wave energy potential.

In terms of depth, the Caspian Sea rises from north to south. Also, the average depth of the northern part is less than 10 meters, and the middle part varies from 180 to 788 meters, and for the southern part of the sea, the depth varies between 960 to 1025 meters.

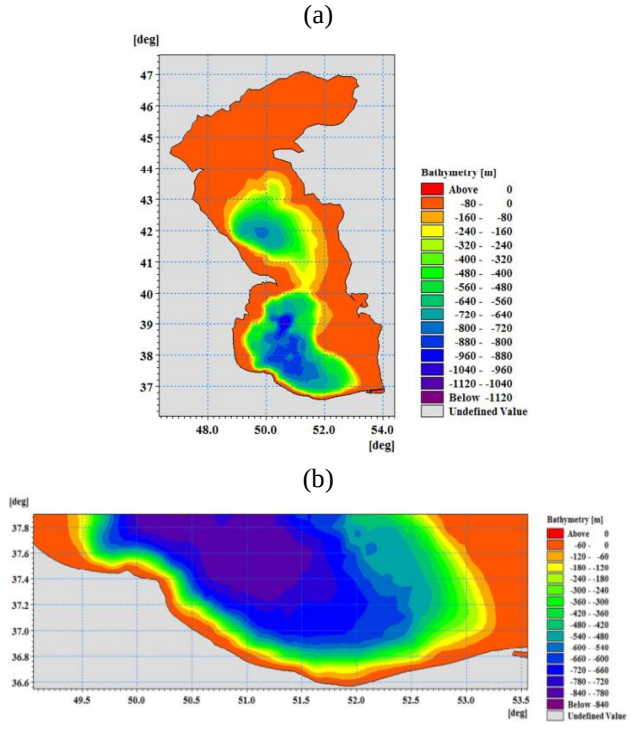

Figure 1. (a) Depth variation in the Caspian Sea.

(b) Magnified view of the variety of depths in the Caspian

Sea[23] According to researches on wave power in the Caspian Sea in different seasons, it has been found

that the wave power is low in spring, which increases slightly in summer. Also, this amount reaches its maximum in autumn and winter. The maximum wave power in autumn is 3.5 kW / m in autumn, and the minimum wave power is 1.5 kW / m in spring[23].

(a)

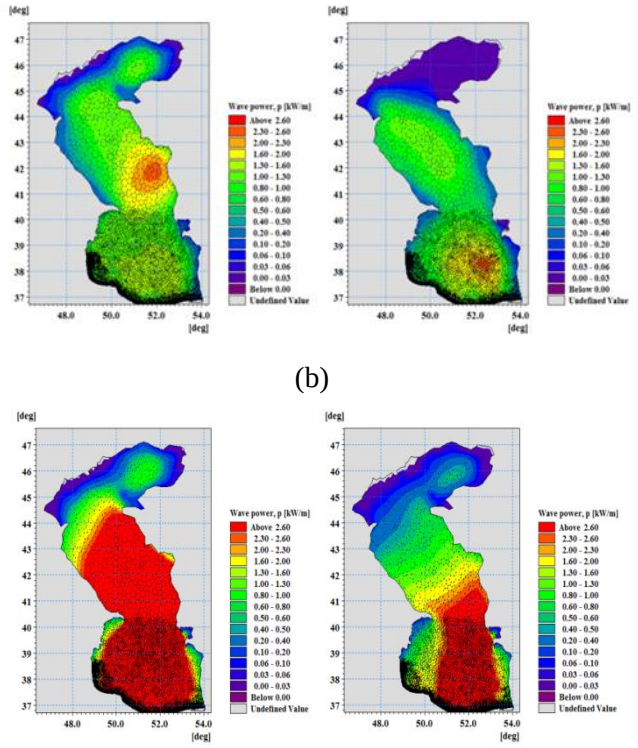

(b)

Figure 2. (a) Wave power in the Caspian Sea in spring (left) and summer (right)

Regarding the wind characteristics in the Caspian Sea, in the southern part of the sea, the number of days with storms (wind speed more than 15 m/s) does not exceed 20 to 30 per year. On the other hand, in the northern parts of the Caspian Sea and the eastern parts of its central section, between 30 and 40 storms are observed annually.

About 10 to 12 percent of the northwest and southeast winds have a speed of about 5 to 9 m/s (moderate wind), which increases somewhat in summer. On the other hand, strong winds at speeds of more than 10 m/s are not more than 4 to 6 percent. But winds of more than 25 m/s are rare and do not exceed a few per year. The average annual wind speed over the entire Caspian Sea is 5.7 m/s. The highest average wind speed of 6 to 7 m/s is observed in the Caspian Sea's central part. On the entire east coast, the average annual wind speed is approximately 5 to 6 m/s, and the maximum is observed on the Mangishlak Peninsula. In the southern Caspian Sea, where strong winds are rare, the average annual wind speed is 4.4 m/s [24].

2. Materials and methods

The model is based on research conducted at the University of Aalborg by j. Kofoed, who has done most of the research on the device[1]. The initial model was made according to the study's dimensions and on a laboratory scale in Solidworks software and transferred to ANSYS workbench software.

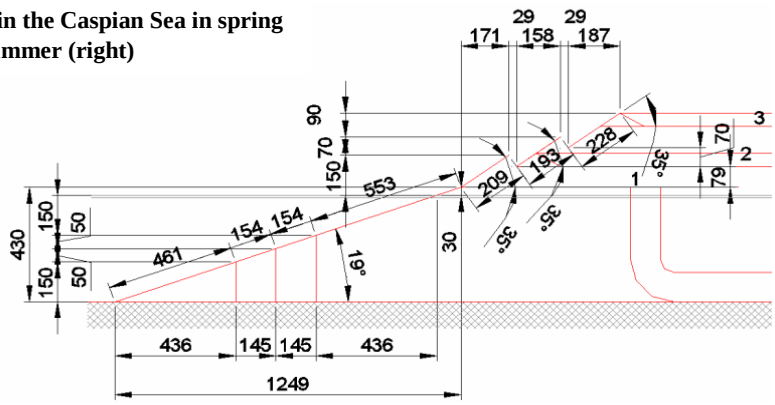

Figure 3. Dimentions provided by j.kofoed[1]

(a)

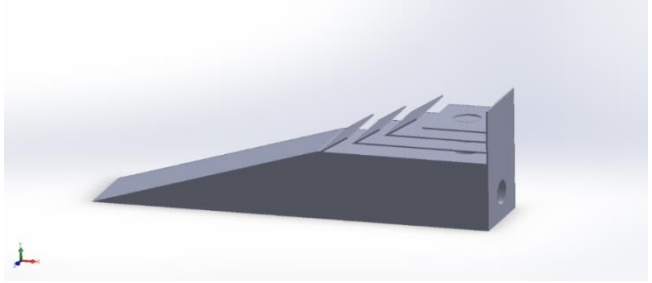

(b)

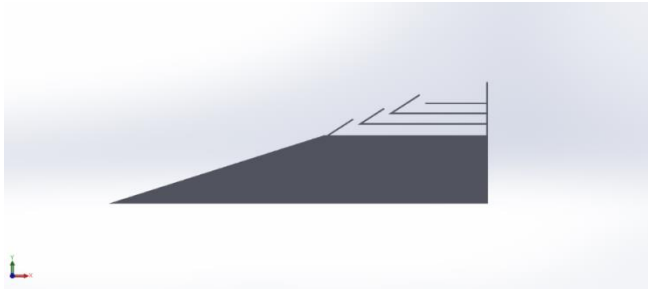

Figure 4. (a), (b) Model made in solidworks software based on research laboratory sizes

But on the other hand, according to Margheriniti's research on this breakwater, one of the things Margheriniti considered when using this breakwater was the issue of water height in front of the structure because things like sediment problems can reduce the efficiency of the system. According to research, the water's height should be at least 15 meters to avoid sediment issues when using this breakwater[9]. On the other hand, this model is designed for a water height of about 6 meters. According to the changes made, this breakwater is about 60 meters long, about 20 meters high, and about 9 meters wide, according to the figure below, without any changes in principal dimensions.

Figure 5. The model is in real size after applying changes to the top in solidworks software

Since the built model is not suitable for simulation and appears as a surface in the ANSYS SpaceClaim, some changes are made in this space on the built model.

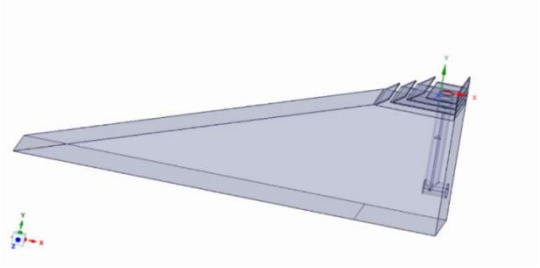

Figure 6. Model after modifications

Finally, the designated sections for water were created in the simulation to prepare the model for data entry.

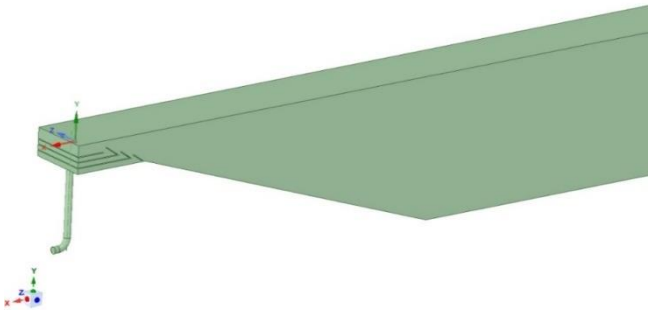

Figure 7. The final model of break water

In the ANSYS meshing, to start in the physics preference section, select the CFD option, and then in the solver preference section, the fluent solver type was placed. Also, the kind of policy used in this study is the Cutcell mesh.

In the next step, naming on different sections and by doing so, various inputs and their types, walls, outputs, etc., were determined.

This study had two types of inputs, Water and air inlet. This model also had two outputs, one of them is the path output installed, and the other is the output of the air part in this model. Another thing was to specify the part where the fluids are in contact with each other, and finally, the other parts were called walls.

With the naming done and each section's name specified, the mesh was inserted for each section with the appropriate size, in such a way that the parts had smaller meshes than the other parts because of their greater importance.

In the model made by creating a body sizing in the mesh settings, the part related to the mix section, a combination of two phases of climate, was applied with more delicate elements in the range of 0.08 meters. Also, for the air part, like the mix part, another body sizing was created, and a mesh with a 0.5-meter element was applied to it, and the other parts have a mesh element with a size of 1 meter.

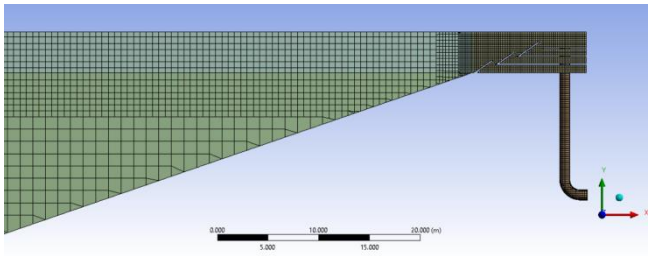

Figure 8. Overview of the created mesh for model

In the ANSYS fluent, the model was imported, and the desired data such as wave specifications and simulation conditions were defined for it. To speed up the simulation, the model was imported in two dimensions in fluent.

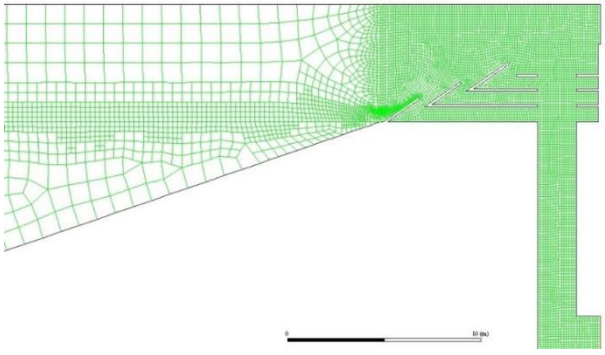

Figure 9. 2D view imported in ANSYS fluent

In this simulation, data from one of the articles related to the South Caspian Sea coasts study have been used. The elevations obtained from the report are 0.06, 0.5, and 2.825, respectively, and the periodicities obtained are 1.7, 4.2, and 8.3, respectively[25]. The following

table provides information on possible scenarios for simulation in Anzali port using that information:

Table1. information about waves for simulation

Wave speed (C)m/s	Wavelength (L)m	Wave period (Ts) s	Wave height (Hs)m	Count possible situations
2.6	4.5	1.7	0.06	(1
2.6	4.5	1.7	0.5	(2
6.56	27.55	4.2	0.06	(3
6.56	27.55	4.2	0.5	(4
6.56	27.55	4.2	2.825	(5
13.02	107.6	8.3	0.06	(6
13.02	107.6	8.3	0.5	(7
13.02	107.6	8.3	2.825	(8

In this study, the vote of a more detailed study of waves, each simulation was performed as a single wave to study each wave's effects on the breakwater more accurately.

The average wave power (W/m) of the SSG wave-energy extraction device can be computed based on the height and period of the wave as:

$$P_{wave=\rho g^2 H_s^2 T_e/64\pi} \quad (1)$$

where r is the water density; g is gravity acceleration; Hs is the significant wave height, and the energy period Te is estimated—here simply set to be Tp/1.15 (Tp: wave peak period). Also, the average potential water overpasses power (W/m) can be computed as:

$$P_{Hyd} = \sum_{j=1}^{n=3} \rho g q_{ov,j} R_{C,J} \quad (2)$$

Where $q_{ov;j}$ is the average volume of incoming water per width in the tank number j, and $R_{c;j}$ is the crest height of the wave in the tank number j, and N_{Res} is the total number of tanks in the SSG breakwater.[3] To calculate $q_{ov;j}$, the following equation has been used.:

$$q_{ov,j} = \int_{R_{c,j}}^{R_{c,j+1}} \frac{dq}{dz} dz = \left(\Pi_j \lambda_j\right) \times \sqrt{g \times H_S^3} \times \frac{A}{B} \times e^{C\frac{R_{C,1}}{H_{m_0,t}}} \times \left[e^{B\times\frac{R_{C,j+1}}{H_{m0,t}}} - e^{B\times\frac{R_{C,j}}{H_{m0,t}}}\right] \quad (3)$$

Parameters A, B, and C in equation (8) are experimental coefficients for a standard design. The geometrical difference between a new design and the standard one can be expressed as the correction coefficient (k_j).

Referring to the previous researches, these empirical coefficients (A, B, and C) can be considered as follows

$$\begin{cases} A = 0.197 \\ B = -1.753 \\ C = -0.408 \end{cases} \quad (4)$$

According to experimental tests, the best $R_{c;j}$ for the reservoir crest height from the sea water level obtained were $R_{c,1}$ = 1.5 m , $R_{c,2}$ = 2.5 m and $R_{c,3}$ = 4.5 m

It should be mentioned that λ_j is also a combination of three different coefficients including discharge coefficient (λ_{dr}), area coefficient ($\lambda_{\alpha r}$), and crest coefficient (λ_s).

$$\lambda_{dr} = 1 - k\frac{Sinh\left(2K_p h\times\left(1-\frac{d_r}{h}\right)\right)+(2K_p h)\times\left(1-\frac{d_r}{h}\right)}{Sinh(2K_p h)+(2K_p h)} \quad (5)$$

In the above-mentioned equation, k is a control coefficient for the incoming wave into the submerged area of the breakwater. It is usually considered to be 0.4. d_r in equation (5) is the distance between average sea level and the lower edge of the lowest breakwater's ramp, and K_p is the maximum wave number of the wave with the maximum wavelength (L_p).

As mentioned, $\lambda_{\alpha r}$ can be derived using equation (6) :

$$\lambda_{\alpha r} = \cos^3(\alpha_r - 30) \quad (6)$$

where α_r is the angle of ramp under mean sea level and its optimal value was considered to be 30°. This value simplifies equation (6) as $\lambda_{\alpha r} = 1.\lambda_s$ coefficient can be obtained using following equation:

$$\lambda_s = \begin{cases} 0.4\ sin\left(\frac{2\pi}{3}R\right) + 0.6 & For\ R < 0.75 \\ 1 & For\ R \geq 0.75 \end{cases} \quad (7)$$

In which $R = R_c / H_s$

The whole mass of water which enters to the SSG breakwater can be calculated from the below experimental formulas

$$\frac{\sum_{j=1}^{N} q_{ov,j}}{\lambda_{\alpha r}\lambda_{dr}\lambda_s\sqrt{gH_{m0,t}^2}} = 0.2 \times e^{-2.6\times\frac{R_{c,j}}{H_{m0,t}}} \quad (8)$$

or

$$Q = \frac{q}{\lambda_{\alpha r}\lambda_{dr}\lambda_s\sqrt{gH_s^3}} = 0.2 \times e^{-2.6\times\frac{R_C\ 1}{H_s\gamma_b\gamma_h\gamma_\beta}} \quad (9)$$

referring to the literatures $\gamma_r = \gamma_b = \gamma_h = \gamma_\beta = 1$.

Koefoed presented a formula as follows

$$\frac{q}{\lambda_{\alpha r}\lambda_{dr}\lambda_s\sqrt{gH_s^3}} = 0.2 \times e^{-2.6\times\frac{R_{c,j}}{H_s}} \quad (10)$$

And the efficiency is calculated from the following equation[15]

$$\eta_{Hyd}^{SS} = {P_{Hyd}}/{P_{wave}} \quad (11)$$

3. Results

3.1. Wave No. 1

This wave has a height of 0.06 meters and a period of 1.7 seconds. Over time, the peak velocity in the contour decreases, and as the wave recedes, the wave velocity gradually decreases. The speed is gradually reduced at the beginning of the path, and the speed is increased at the output channel. Also, over time, the speed at the output path decreases, and its value decreases. This reduction is also observed along the channel path.

As time goes on and the wave recedes, the volume of available water decreases, and the peak point of the wave occurs before 15 seconds; and the first and second reservoirs are emptied, and the third reservoir is emptied. In general, in this wave, due to the smaller volume of water, most of the lower reservoirs are involved, and the upper reservoirs, especially the first reservoir, do not pass a large volume of fluid.

As shown in the diagram, the end of the diagram is when the fluid enters the outlet path, which is naturally accompanied by an increase in velocity and energy. In the first graph of fluid velocity, we see that the fluid has a constant velocity for most of the simulation time. When it enters the output channel, it reaches its maximum velocity of about 12 m / s for a moment.

(a)

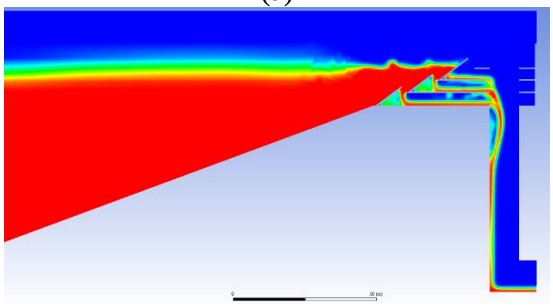

(b)

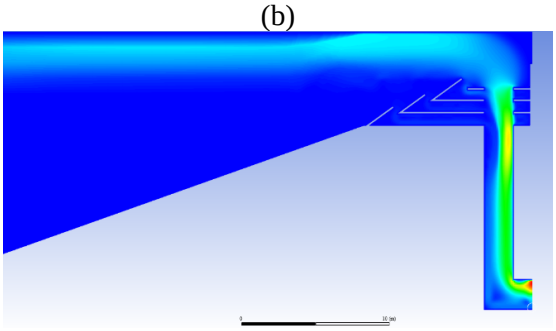

(c)

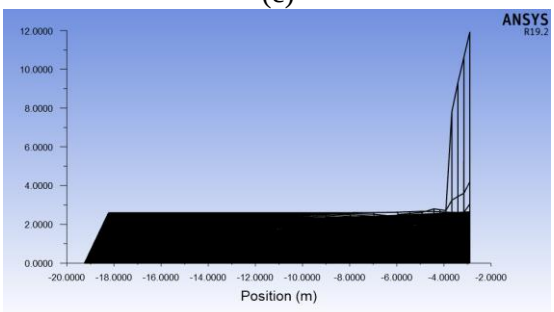

Figure 10. (a) The volume of water for wave No. 1. (b) Velocity situation in wave No. 1,(c) Velocity chart for wave No. 1

This mode has an average speed of 2.2 m/s, wave power of 0.00293 kW/m, and hydraulic efficiency of 0.099 kW/m.

3.2. Wave No. 2

This wave has a height of 0.06 meters and a period of 4.2 seconds. Over time, we see a gradual decrease in the speed of the output path. However, this reduction is more noticeable along the output path and is not detectable in the channel's end parts due to involvement until the last moment.

Because the first and second waves have the same velocity of 2.6 m/s, they are almost equal in terms of inlet water volume and shapes and differ only in some details.

According to the information in the diagram of the water flow velocity, it can be seen that in a wave with these conditions, the maximum velocity can reach about 16 meters per second. Still, in other cases, the fluid velocity is a constant value.

(a)

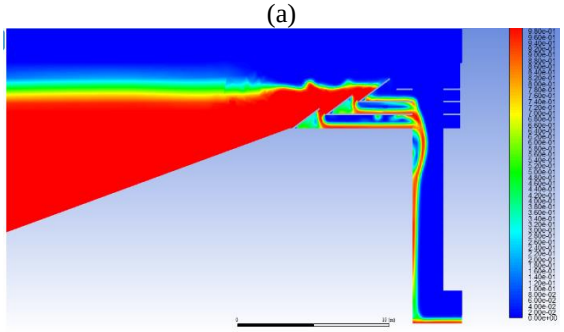

(b)

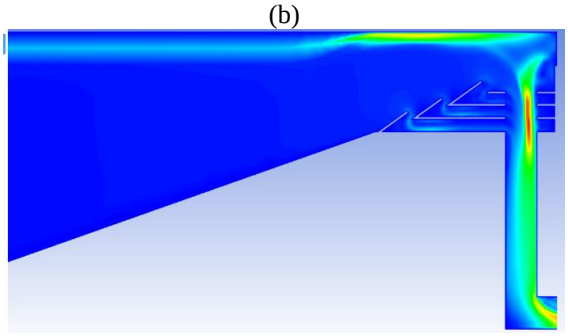

(c)

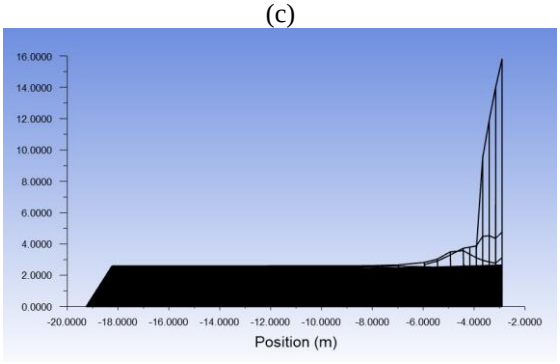

Figure 11. (a) the volume of water for wave No. 2. (b) velocity situation in wave No. 2. (c) velocity chart for wave No. 2

This mode has an average speed of 2.15 m/s, wave power of 0.20352 kW/m, and hydraulic efficiency of 0.06326 kW/m.

3.3. Wave No. 3

The increase in velocity is visible from the air and water phases. Also, to a limited extent, an increase in water inlet speed can be seen in the lower reservoir. Due to the increase in velocity and the increase in water volume, more time is needed to drain the water, which makes the descent of the deceleration, in this case, have less night. On the other hand, due to the higher speed in the third wave, we see a noticeable increase in speed at the output of the three reservoirs and the wall of the output channel. However, over time, this speed is transmitted to the output channel relative to 8 seconds. On the other hand, due to the increase in water volume, we are witnessing changes in the reservoirs' inlet velocities.

As shown in the figure, due to the increase in velocity, the water volume has increased and completed more of the breaking capacity, but not completely. On the other hand, it can be seen that the volume of water in the canal is gradually draining from 8 to 15 seconds. Furthermore, when the channel empties of fluid, a slight instability is observed over the simulation time**.**

As can be seen in the flow velocity diagram, the main velocity is related to the same velocity of 6.52 m/s, which reaches its maximum value of about 8 to 9 m/s when entering the output channel.

(a)

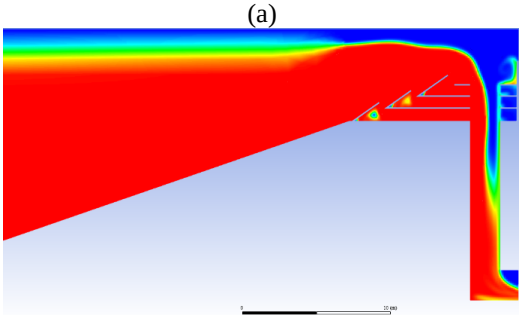

(b)

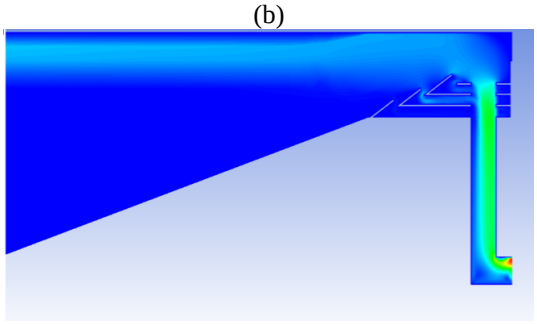

(c)

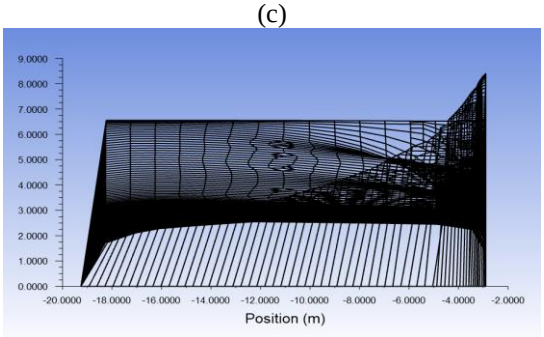

Figure 12. (a) the volume of water for wave No. 3. (b) velocity situation in wave No. 3. (c) velocity chart for wave No. 3

This mode has an average speed of 2.7 m/s, wave power of 0.00724 kW/m, and hydraulic efficiency of 0.097062 kW/m.

3.4. Wave No. 4

In the relevant image of 8 seconds, we see the speed spread throughout the channel wall. But moving to higher seconds of the simulation, we see a decrease in water's speed entering the reservoirs. We also see velocity pressure at the inlet point of the reservoirs to the outlet channel. Due to the similarity of velocity to the third wave, the velocity contour is similar to the third wave contour. As in the output of the reservoirs and the channel wall, we see a high number of velocities, which are reduced by continuing the simulation process. And is broadcast throughout the channel.

At second 8, a slightly larger water volume enters the channel than at second 8 of the third wave. But in the 15th second, as the wave recedes, we see a decrease in the water in this breakwater output path.

In the flow velocity diagram, similar to the third wave, most of the simulations have a constant velocity at the beginning of the simulation, which is 6.25 m/s, reaching its maximum value of about 8 m/s by entering the reservoirs and the output channel.

(a)

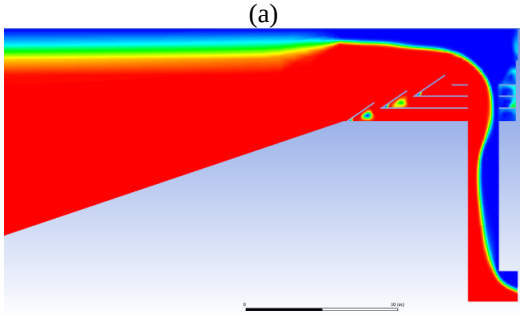

(b)

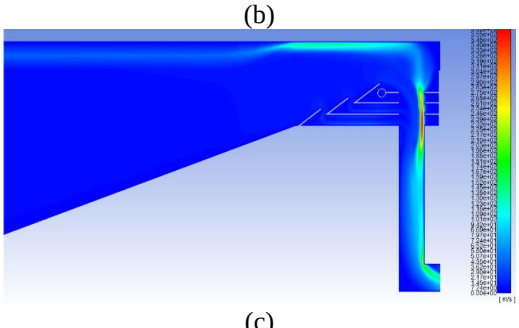

(c)

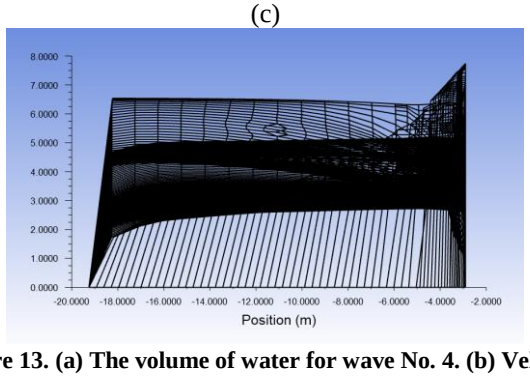

Figure 13. (a) The volume of water for wave No. 4. (b) Velocity situation in wave No. 4.(c). Velocity chart for wave No. 4

This mode has an average speed of 2.72 m/s, wave power of 0.50282 kW/m, and hydraulic efficiency of 0.07296 kW/m.

3.5. Wave No. 5

In this case, unlike other cases, there is no regular entry and exit of water fluid, and turbulence at the inlet is well known, especially in the 8th second. We cause part of the water to pass from the breakwater to the space behind the water. Also, this turbulence on different parts of this breakwater, such as the speed of water entering the reservoirs, is significant. But by going through this step to higher seconds, the simulation is balanced, and the input speed of the reservoirs is almost the same as the previous two modes. On the other hand, the velocity turbulence in the output channel, which we saw in 8 seconds, has reached a normal equilibrium in this second. Most of the velocity is visible in certain areas, such as the output of the reservoirs. It should be noted that, unlike the previous two waves, which had points with an accumulation of velocity in the 8th second, in this wave, this state occurred later, and in the 15th second, we see this issue.

In the flow volume contour, the amount of turbulence created and the water volume that the breakwater has passed can be seen, which is 15th seconds; as the water flow reaches equilibrium and the wave recedes, the volume of water in the breakwater gradually decreases. As in the previous waves, the regression and stability of the fluid flow can be seen.

In the flow velocity diagram, the simulation starts with the input number of 6.25 m/s, mostly stable. Only at the beginning of the reservoirs in which we saw turbulence, we see some increase. Finally, we see water entering the canal, which is a maximum of about. It reaches 12 m/s.

(a)

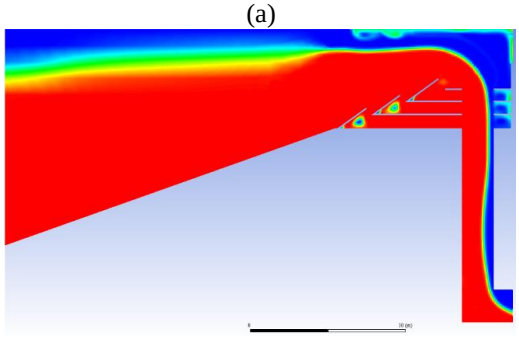

(b)

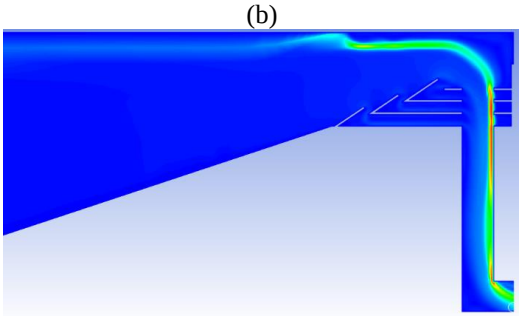

(c)

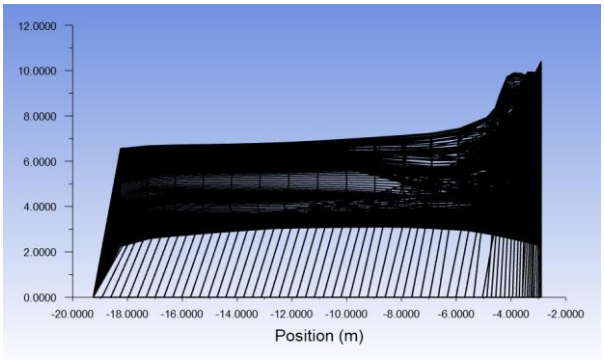

Figure 14. (a) The volume of water for wave No. 5. (b) Velocity situation in wave No. 5. (c) Velocity chart for wave No. 5

This mode has an average speed of 2.81 m/s, wave power of 16.05164 kW/m, and hydraulic efficiency of 0.58104 kW/m

3.6. Wave No. 6

Due to the high speed of the wave, we see the arrival of a large volume of water and, in fact, the use of all the capacity of the breakwater, which leads to an increase in the overall speed in various parameters of the breakwater. This wave has a higher speed in the simulation stages than the previous waves, which causes the speed to have large values along the output channel. Also, input speed values have been increased. Over time, we see an increase in speed in the outlet channel, which due to the large volume of water, it is natural that it takes longer. Of course, the highest speed can be seen on the sides of the channel and the channel output.

Due to the high velocity of the wave and the arrival of a large water flow volume, it was clear that all paths were full. Naturally, due to this amount of fluid volume, even with the wave retreating, it takes longer than in other cases for the fluid to flow from the outlet. Be evacuated. Due to the high volume of water, more time is needed for the wave to retreat. Although. At 15 seconds, there are signs of a wave reversal.

In the velocity diagram, during the simulation, it has an almost constant velocity equal to the incoming velocity of 13.02 m/s. Gradually, however, as the simulation progresses, this value increases to a maximum of about 30 m/s.

(a)

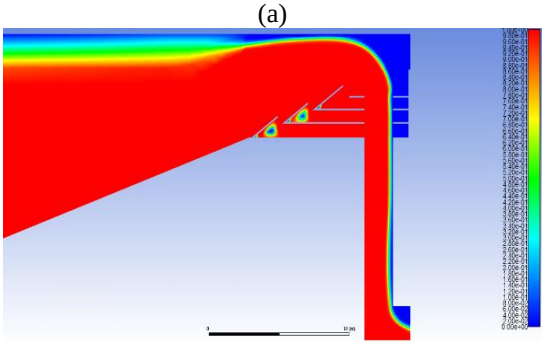

(b)

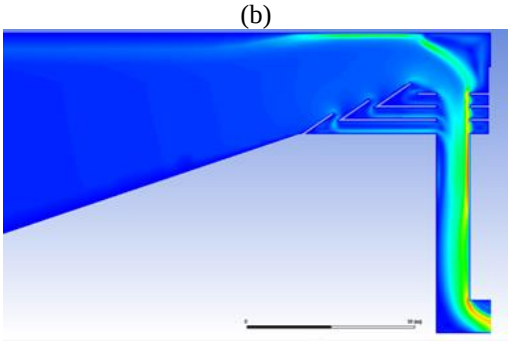

(c)

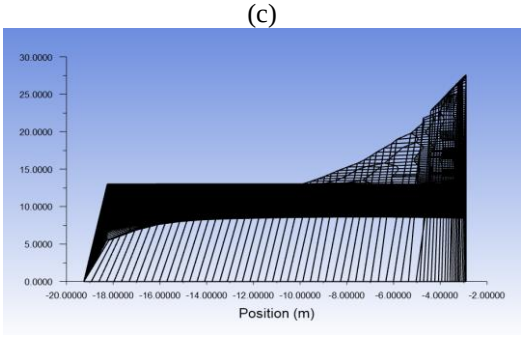

Figure 15. (a) The volume of water for wave No. 6. (b) Velocity situation in wave No. 6. (c) Velocity chart for wave No. 6

This mode has an average speed of 6.1 m/s, wave power of 0.01430 kW/m, and hydraulic efficiency of 0.01773 kW/m

3.7. Wave No. 7

Similar to the sixth case, due to the same speed, in this case, too, a large volume of water fills the outlet path, and no significant change is seen in the figure, such as turbulence. Similar to the previous cases, at the point of exit of water fluid into the outlet channel, we see the highest velocity as a point that is a combination of air and water velocity. Also, in 15 seconds, we see a faster scatter than in 8. Due to the velocity similar to the sixth wave, the velocity contour of the seventh wave is identical to the sixth wave, and we see the maximum velocity at the side of the channel as well as at the output in 8 seconds, which increases throughout the channel as the simulation time.

According to the previous explanation, which is also evident here, a large volume of water flow almost fills the outlet path's capacity. It requires more time than other cases to empty this volume of water fluid. Also, we see the gradual balancing of the input wave and the beginning of its regression.

According to the diagram, the speed, in this case, has reached about 30 m/s; although similar to the previous wave, most of the simulation time has remained constant, but in the end, has increased.

(a)

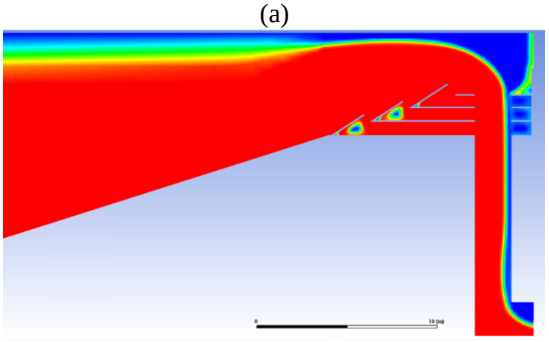

(b)

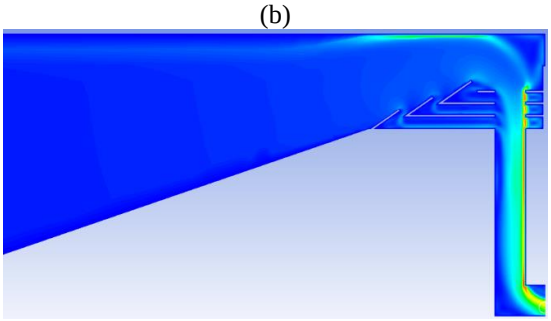

(c)

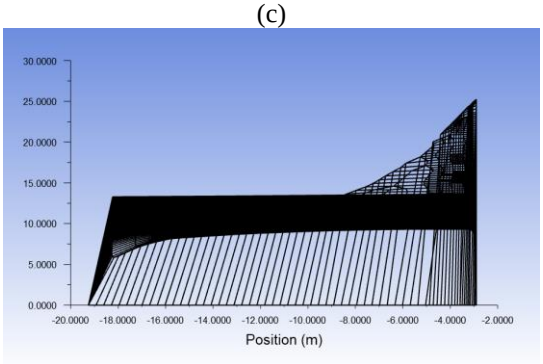

Figure 16. (a) The volume of water for wave No. 7. (b) Velocity situation in wave No. 7. (c) Velocity chart for wave No. 7

This mode has an average speed of 6.3 m/s, wave power of 0.99367 kW/m, and hydraulic efficiency of 0.6136 kW/m

3.8. Wave No. 8

Due to its speed equal to the previous two modes, it has a similar distribution. As the simulation process continues, this speed begins to reach equilibrium, and its scattering decreases. On the other hand, the speed of water entering the reservoirs is also reduced. As a result, instead of the speed distribution in the channel being uniform, we see an increase in this value at the side of the channel and the outlet of the reservoirs, which continues to the outlet of the channel.

As in the previous two cases, at a speed of 13.02 m/s, the volume of flowing water fills the entire path. Also, according to this mode's information, the eighth mode has the highest intensity among other modes. However, as the simulation process continues, water volume gradually decreases, as shown in the 15th second image.

In the diagram of fluid flow velocity, most simulation time has a constant input time of 13.02 m / s. But with the arrival of the reservoirs and the entry of fluid flow

into the outlet channel, this value has increased and reached it maximun valie.

(a)

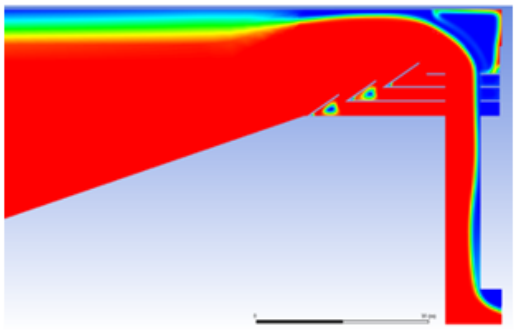

(b)

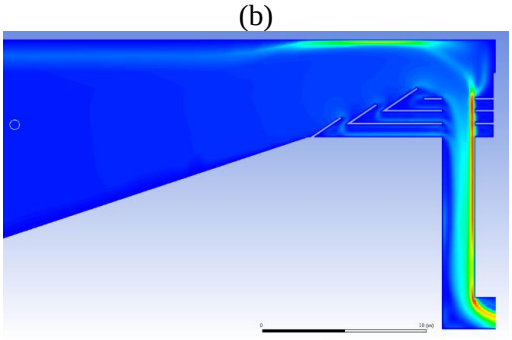

(C)

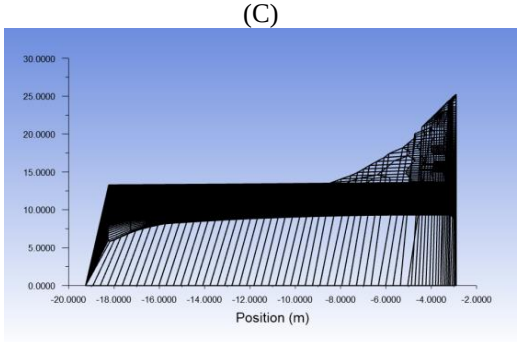

Figure 17. (a) The volume of water for wave No. 8. (b) Velocity situation in wave No. 8. (c) Velocity chart for wave No. 8

This mode has an average speed of 6.71 m/s, wave power of 31.72074 kW/m, and hydraulic efficiency of 0.86550 kW/mc

3.9. Validation

To confirm the method's accuracy to obtain the numbers used in this study, validation was performed based on valid research. In this work, based on the dissertation done in this direction in the country's southern seas[26], a criterion was set in which the study is both modelings using FLOW 3D software for different waves and examining laboratory behaviour and comparison of the respective breaker. Accordingly, a wave with a periodicity of 1.84 seconds and a wave index height of 0.069 m was considered, simulated in ANSYS fluent software, and the corresponding numbers were obtained. Also, by equating the number obtained in FLOW 3D software for the same conditions, the software

Table 2. Information of validation

H_S (m)	0.069
T_P (s)	1.84
V_M (Flow3D)	1.90
V_M (Ansys)	2.26
Error	%18.9

number for the average speed obtained in ANSYS fluent software is 2.26 m/s, and the desired number for FLOW 3D software is 1.90 m/s,which is a difference of 18.9%. Show that it is a relatively acceptable error.

4. Discussion

According to the information in this table, it is clear that this breakwater's efficiency is a deficient number and is out of the economic range for most waves with a height of less than one meter.

Also, for waves with a height of more than one meter and a period of more than 4.2 seconds, good efficiency can be observed. In general, the highest efficiency expected from this system in the Caspian Sea is the eighth wave with a height of 2.825 meters and a period of 8.3 seconds, which has an efficiency of about 86%.

The following diagrams show the changes in wave height and the changes in the waves' periodicity over about three months in 2019, prepared by the Ports and Shipping Authority.

Table 3. shows an overview of the results obtained from the simulation of the eight selected waves

Type of Spectrum	1	2	3	4	5	6	7	8
Tp (s)	1.7	1.7	4.2	4.2	4.2	8.3	8.3	8.3
Hs (m)	0.06	0.5	0.06	0.5	2.825	0.06	0.5	2.825
V_{mean} (m/s)	2.2	2.15	2.70	2.72	2.81	6.10	6.30	6.71
P_{wave} (kW/m)	0.00293	0.20352	0.00724	0.50282	16.05146	0.01430	0.99367	31.72074
P_{Hyd} (kW/m)	0.00029	0.01287	0.00070	0.03668	9.32654	0.00025	0.60971	27.45430
η^{ss}_{Hyd}	0.099	0.063	0.097	0.072	0.581	0.017	0.613	0.825

(a)

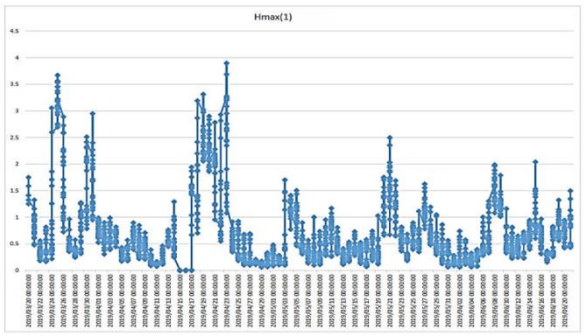

(b)

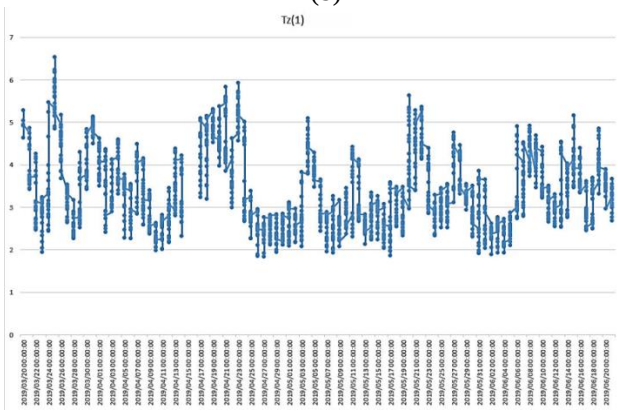

Figure 18. (a) Graph of wave height occurring in 100 days (b) Graph of wave period occurring in 100 days

According to the information obtained from these diagrams, it is clear that the principal height of the waves in the Caspian Sea is about 0.5 meters and less. Also, the periodicity is about 3 to 4 seconds.

But among the three waves that are most efficient than the others, in this period, we see only the fifth wave and the seventh and eighth waves did not occur, and their occurrence in the Caspian Sea is unlikely.

5. Conclusion

In this study, the possibility of using SSG breakwaters on the southern shores of the Caspian Sea and, more precisely, the Bandar Anzali region was investigated. First, the Caspian Sea's general characteristics, such as the characteristics of waves and wind currents in the sea, were examined. Then, according to previous research in this field, its model was built in ANSYS software. Also, simulations were performed in ANSYS fluent. Based on the available information, eight waves were selected, and for each wave in specific factors such as total pressure, velocity, current volume, and other cases were examined.

Regarding the possibility of using this breakwater, considering that most of the waves in the time shown are close to the simulated wave No. 4, and given that waves with a height of less than 1 meter of sufficient efficiency are not available, Therefore, it is recommended to use this system in smaller dimensions, which are more economically viable.

Author Contributions:

Hereby, it is confirmed that all the authors contributed in the manuscript.

References

[1] Kofoed, J.P., *Model testing of the wave energy converter Seawave Slot-Cone Generator*. Hydraulics and Coastal Engineering, 2005(18).

[2] Larsen, B.J. and J.P. Kofoed, *Model Test Setup and Program for Experimental Estimation of Surface Loads of the SSG Kvitsøy Pilot Plant from Extreme Wave Conditions.* Hydraulics and Coastal Engineering, 2005(32).

[3] Margheritini, L., J.P. Kofoed, and P. Frigaard, *Status and performance of the SSG Wave Energy Converter*. Department of Civil Engineering, Aalborg University, Denmark, 2006.

[4] Kofoed, J.P., D. Vicinanza, and E. Osaland. *Estimation of design wave loads on the SSG WEC pilot plant based on 3-D model tests*. in *The Sixteenth International Offshore and Polar Engineering Conference*. 2006. International Society of Offshore and Polar Engineers.

[5] Jensen, P.M., L. Gilling, and J.P. Kofoed, *User manual for SSG power simulation 2.* 2006.

[6] Beseau, M., *Analysis o f Computational Fluid Dynamics study on Seawave Slot-Cone Generator.* 2006.

[7] Margheritini, L. and A. Morris, *Model tests on overall forces on the SSG pilot plant.* 2007.

[8] Borgarino, B. and J.P. Kofoed, *Power Production from Integration of SSG in a Breakwater at Liseleje.* 2007.

[9] Margheritini, L., D. Vicinanza, and P. Frigaard, *SSG wave energy converter: Design, reliability and hydraulic performance of an innovative overtopping device.* Renewable Energy, 2009. 34(5): p. 1371-1380.

[10] Alamian, R., et al., *Evaluation of technologies for harvesting wave energy in Caspian Sea.* Renewable and Sustainable Energy Reviews, 2014. 32: p. 468-476.

[11] Oliveira, P., et al., *Experimental evaluation of the effect of wave focusing walls on the performance of the Sea-wave Slot-cone Generator.* Energy Conversion and Management, 2016. 110: p. 165-175.

[12] Buccino, M., et al., *The use of CFD in the analysis of wave loadings acting on seawave slot-cone generators.* Sustainability, 2016. 8(12): p. 1255.

[13] Musa, M.A., et al., *Numerical simulation of wave flow over the overtopping breakwater for energy conversion (OBREC) device.* Procedia engineering, 2017. 194: p. 166-173.

[14] Maliki, A.Y., et al., *Comparison of numerical and experimental results for overtopping discharge of*

the OBREC wave energy converter. J. Eng. Sci. Technol, 2017. 12(5): p. 1337-1353.

[15] Salimi, F., M. Rahbani, and B. Mohammadi, *Feasibility assessment for installing Sea-wave Slot-cone Generator breakwater in the Iranian coasts of Persian Gulf and Oman Sea*. Energy & Environment, 2018. 29(1): p. 95-108.

[16] Rodriguez-Delgado, C., R.J. Bergillos, and G. Iglesias, *Dual wave farms for energy production and coastal protection under sea level rise*. Journal of Cleaner Production, 2019. 222: p. 364-372.

[17] Di Lauro, E., et al., *Advantages of an innovative vertical breakwater with an overtopping wave energy converter*. Coastal Engineering, 2020: p. 103713.

[18] Hernández-Fontes, J.V., et al., *Is ocean energy an alternative in developing regions? A case study in Michoacan, Mexico.* Journal of Cleaner Production, 2020. 266: p. 121984.

[19] Gonçalves, M., P. Martinho, and C.G. Soares, *Wave energy assessment based on a 33-year hindcast for the Canary Islands.* Renewable Energy, 2020. 152: p. 259-269.

[20] Ribal, A., et al., *A high-resolution wave energy resource assessment of Indonesia.* Renewable Energy, 2020. 160: p. 1349-1363.

[21] Alizadeh, M.J., et al., *Projection of spatiotemporal variability of wave power in the Persian Gulf by the end of 21st century: GCM and CORDEX ensemble*. Journal of Cleaner Production, 2020. 256: p. 120400.

[22] Jahangir, M.H., A. Shahsavari, and M.A.V. Rad, *Feasibility study of a zero emission PV/Wind turbine/Wave energy converter hybrid system for stand-alone power supply: A case study*. Journal of Cleaner Production, 2020. 262: p. 121250.

[23] Jahangir, M.H. and M. Mazinani, *Evaluation of the convertible offshore wave energy capacity of the southern strip of the Caspian Sea.* Renewable Energy, 2020. 152: p. 331-346.

[24] Kosarev, A.N., *Physico-geographical conditions of the Caspian Sea*, in *The Caspian Sea Environment*. 2005, Springer. p. 5-31.

[25] Alamian, R., et al., *Wave energy potential along the southern coast of the Caspian Sea*. International journal of marine energy, 2017. 19: p. 221-234.

[26] Khalifehei, K., G. Azizyan, and C. Gualtieri, *Analyzing the Performance of Wave-Energy Generator Systems (SSG) for the Southern Coasts of Iran, in the Persian Gulf and Oman Sea.* Energies, 2018. 11(11): p. 3209.